Narrowband and Wideband Dual-Mode Wireless Power Transfer System with a Single Transmitter

Enes Ayaz, Ogün Altun, Ozgur Gulsuna, Ozan Keysan

***Abstract*—This study introduces a dual-mode wireless power transfer (WPT) system for multi-standard wireless charging products. The system allows two receivers to operate concurrently at narrowband and wideband frequencies using the proposed sinusoidal pulse width modulation (SPWM). Conventional SPWM does not provide independent control of switching and sideband harmonics, which are required for dual-mode excitation. We propose a new hybrid carrier and reference phase shift method to provide independent control of the reference, switching, and sideband harmonics. A prototype has been developed to validate power transfer at both narrowband (951 kHz and 1190 kHz) and wideband (100 kHz and 1190 kHz) frequency operations.**

***Index Terms*—Wireless power transfer, dual-mode wireless power transfer, SPWM, multi-standard wireless charging**

I. Introduction

Recent developments in wireless power transfer (WPT) technologies have encouraged wireless charging devices in robotics and consumer electronics [1]. Various WPT standards that regulate commercial devices have also given opportunities for WPT systems to spread in these applications. One of the most common standards is Qi by the Wireless Power Consortium (WPC) [2]. In this standard, 110-205 kHz operating frequency range is adopted for low-power devices (5-15 W) [3]. In addition, 80-300 kHz operating frequency range is specified for medium-power (30-65 W) applications [4]. On the other hand, the Alliance for Wireless Power (A4WP) supports power transfer below 30 W in the operating frequency of 6.78 MHz with $\pm$15 kHz control range, and Power Matters Alliance (PMA) permits power below 5 W in the operating frequency range of 277-357 kHz [3], [5], [6]. Other frequency bands can also be utilized in various devices. For instance, 300-500 kHz range can be used in consumer devices for up to 5 W power.

The main advantages of WPT systems are increased safety and portability of the devices. In addition to these advantages, another benefit of wireless charging is its potential ability to charge multiple devices simultaneously using a single transmitter. For instance, it could wirelessly charge simultaneously several mobile phones and headphones from different manufacturers on a single pad. This capability has the potential to reduce costs and save space. However, at this point, it's significant to note that current standards for wireless charging are not universal and compatible. The lack of interoperability due to this incompatibility poses a challenge when desiring to utilize a single device with multiple products. Therefore, achieving interoperability among these standards would result in cost savings and making wireless charging widespread. For this aim, WPT systems with single-transmitter (single-Tx) and dual-receivers (dual-Rx) gain popularity [7]–[14].

These systems utilize multiple coils and a dual-frequency inverter; thus, they can transmit power at two frequencies, which can be categorized as wideband and narrowband, according to their different operating frequencies. Wideband and narrowband systems differ significantly. Narrowband systems operate at closely spaced frequencies, presumably within the same standard. Wideband systems operate over a broader frequency range, encompassing signals from widely spaced frequencies and presumably different standards.

In [7], a dual-mode system is introduced to make the Tx device compatible with two WPT standards of A4WPT (6.78 MHz) and WPC/PMA (200 kHz). However, two set of coils and drivers are used in this system, increasing the complexity and cost. In [8], a single-inverter-based dual-frequency WPT system is proposed using the programmed PWM method, which provides both narrowband and wideband operations. However, this method is computationally complex and requires offline algorithms, which is not feasible for dynamic systems. In [12], time multiplication method is proposed to achieve power transfer at 100 kHz, 200 kHz, and 300 kHz by sequentially enabling the receivers. However, it requires negative gate voltages to avoid the reverse conduction of GaN switches. In [13], multi-frequencies are achieved by comparing superimposed sinusoidal reference signals with high-frequency triangular carrier signals. However, in this method, the switching frequency is higher than the operating frequency of the WPT system, which increases the switching losses. In [14], multi-frequency operation is achieved by a multi-level inverter (MLI) with a switching frequency lower than its two-level alternatives. However, this system uses a higher number of switching components, and it can be utilized in just narrowband operation. In this study, concurrent power transfer at dual-frequency (multi-standards) is achieved by a single converter which is driven by a novel dual-frequency modulation technique. The proposed system can be applied to both narrowband and wideband operations. The main contribution of the study can be listed as follows:

1) A single converter is utilized to achieve a multi-standard concurrent wireless power transfer system, reducing the system's cost.
2) The novel modulation method is easily implemented without extra computational burden.
3) The proposed system can be applied to both narrowband and wideband operations.
4) The proposed method guarantees that the switching frequency is near the operating frequencies, reducing the switching losses.

II. System Structure and Proposed Method

The proposed system is versatile and can work with various topologies. Fig. 1 shows a dual-mode WPT system configuration. In this system, a full-bridge (FB) converter generates dual-frequency output voltages that excite the single Tx coil.

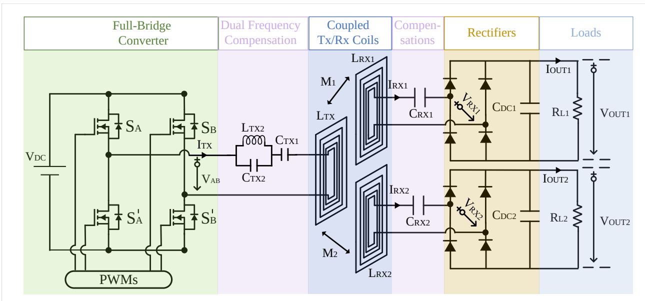

Fig. 1. A representative example of the proposed dual-mode WPT system.

Since the Tx side should let both frequencies to pass through, a dual-frequency compensation circuit is introduced, which will be explained later, while the Rx sides are compensated by only series capacitors. Therefore, Rx coils become selective and operate at different frequencies: f_1 and f_2.

A. Dual Frequency Strategy using SPWM

Conventionally, sinusoidal pulse width modulation (SPWM) is generated by comparing a high-frequency carrier (switching) signal and a reference (fundamental) signal. Its harmonic distribution can be calculated using double Fourier series analysis, as given in (1) where ω_R, ω_C, θ_R, θ_C, are angular frequencies and phases of reference and carrier signals, and J_o, J_k are the zeroth and k^{th} order Bessel functions.

$$\begin{aligned} S &= \frac{1}{2} + \frac{m_a}{2}\cos\Big(\omega_R t + \theta_R\Big) \\ &+ \frac{2}{\pi}\sum_{i=1}^{i=\infty} J_o\Big(i\frac{\pi}{2}m_a\Big)\sin\Big(i\frac{\pi}{2}\Big)\cos\Big(i(\omega_C t + \theta_C)\Big) \\ &+ \frac{2}{\pi}\sum_{i=1}^{i=\infty}\sum_{k=-\infty}^{k=\infty}\left[\begin{array}{c} \frac{1}{i}J_k\Big(i\frac{\pi}{2}m_a\Big)\sin\Big((i+k)\frac{\pi}{2}\Big) \\ \cos\Big(i(w_C t + \theta_C) + k(w_R t + \theta_R)\Big)\end{array}\right] \end{aligned} \tag{1}$$

Although utilizing only reference signals is a common practice, in this paper, it is proposed that switching and sideband harmonics can also be utilized to achieve dual-frequency WPT systems. The magnitudes of reference, carrier, and sideband harmonics for the SPWM scheme are shown in Fig. 2. Hence, in a conventional SPWM scheme, the magnitude of the fundamental signal can be adjusted by the modulation index (m_a), whereas the magnitudes of other components also change with m_a. However, dual-mode WPT systems require independent and concurrent control of two separate frequencies. Accordingly, additional control parameters should be introduced if the components of switching and its sideband harmonics are utilized.

B. The Proposed Control Method

In the proposed method, a hybrid carrier and a reference phase shift control are applied to the SPWM method so that independent dual-frequency at the output voltage of the full-bridge converter can be achieved. The proposed modulation scheme is shown in Fig. 3 where separately controlled carrier and reference signals generate the node A and the node B voltages.

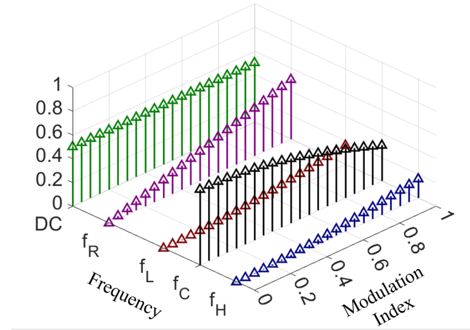

Fig. 2. The normalized magnitudes of the reference, carrier, and sideband harmonics with varying modulation index for the SPWM scheme (for a single leg).

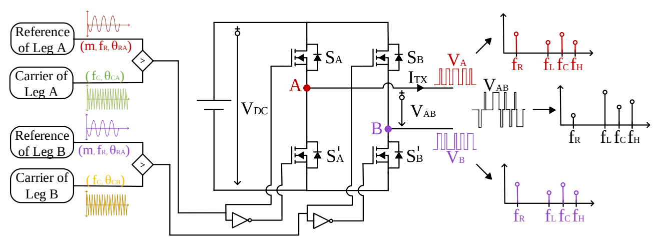

Fig. 3. The proposed modulation scheme of the hybrid control.

The normalized output voltages (over DC-link voltage) for each frequency component (reference ($V_{AB^{f_R}}$), lower-sideband ($V_{AB^{f_L}}$), carrier ($V_{AB^{f_C}}$), and higher-sideband ($V_{AB^{f_H}}$)) can be calculated as in (2), (3), (4), and (5) by using the switching function in (1) with taking ($i=0,\ i=1$), ($i=1,\ k=-2$), and ($i=1,\ k=2$), and using different carrier and reference phases.

$$V_{AB^{f_R}}(t) = \frac{m_a}{2}\Big[cos(\omega_R t + \theta_{R_A}) - cos(\omega_R t + \theta_{R_B})\Big] \tag{2}$$

$$\begin{aligned} V_{AB^{f_L}}(t) = \frac{2}{\pi}J_2(\frac{\pi}{2}m_a)\Big[&cos(\omega_C t - 2\omega_R t + \theta_{C_B} - 2\theta_{R_B}) \\ &- cos(\omega_C t - 2\omega_R t + \theta_{C_A} - 2\theta_{R_A})\Big] \end{aligned} \tag{3}$$

$$\begin{aligned} V_{AB^{f_C}}(t) = \frac{2}{\pi}J_o(\frac{\pi}{2}m_a)\Big[&cos(\omega_C t + \theta_{C_A}) \\ &- cos(\omega_C t + \theta_{C_B})\Big] \end{aligned} \tag{4}$$

$$\begin{aligned} V_{AB^{f_H}}(t) = \frac{2}{\pi}J_2(\frac{\pi}{2}m_a)\Big[&cos(\omega_C t + 2\omega_R t + \theta_{C_B} + 2\theta_{R_B}) \\ &- cos(\omega_C t + 2\omega_R t + \theta_{C_A} + 2\theta_{R_A})\Big] \end{aligned} \tag{5}$$

It is observed that the magnitudes of these components can be adjusted independently by controlling the phases of reference and carrier signals. The control parameters and their affecting components are shown in Table I.

TABLE I
CONTROL PARAMETERS AND OPERATIONS OF SPWM COMPONENTS

Control Parameter	V_{ABf_R}	V_{ABf_L}	V_{ABf_C}	V_{ABf_H}
Modulation Index (m_a)	±	±	±	±
Reference Phase (θ_R)	±	±	0	±
Carrier Phase (θ_C)	0	±	±	±
Operation	V_{ABf_R}	V_{ABf_L}	V_{ABf_C}	V_{ABf_H}
Wideband operation	Selected	-	Selected	-
Narrowband operation-I	-	Selected	Selected	-
Narrowband operation-II	-	-	Selected	Selected

±: can be changed by the control parameter.
0: cannot be changed by the control parameter.

Now, selecting any two frequencies respecting the operation of narrowband or wideband is required as follows:

1) **Wideband operation:** The reference component can be used as the lower frequency, and the carrier component can be used as the higher frequency.
2) **Narrowband operation-1**: The lower-sideband component can be used for the lower frequency and the carrier component can be used for the higher frequency.
3) **Narrowband operation-2:** The carrier component can be used for the lower frequency and the higher-sideband component can be used for the higher frequency.

C. Narrowband Operation

Although there are two options in the narrowband operation, in this section, the f_L and f_C are utilized to achieve dual-frequency of f_1 and f_2, and it is assumed that f_1 is the lower one. The reference and carrier signals should be $f_R = \dfrac{f_2 - f_1}{2}$ and $f_C = f_2$, respectively. The peak value of the components at f_l and f_c can be calculated in phasor domain by using (3) and (4) as given in (6) and (7) where $\Delta\theta_C = \theta_{CA} - \theta_{CB}$, and $\Delta\theta_R = \theta_{RA} - \theta_{RB}$.

$$\hat{V}_{ABf_L} = V_{DC}\frac{2}{\pi}J_2(\frac{\pi}{2}m_a)\sqrt{1-cos(\Delta\theta_C - 2\Delta\theta_R)} \quad (6)$$

$$\hat{V}_{ABf_C} = V_{DC}\frac{2}{\pi}J_o(\frac{\pi}{2}m_a)\sqrt{1-cos(\Delta\theta_C)} \quad (7)$$

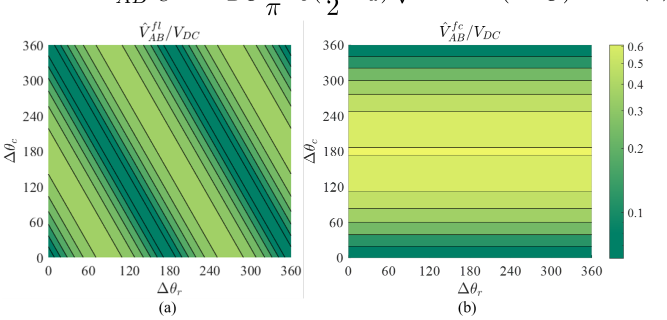

Fig. 4. Narrowband Operation. a) The normalized voltage at f_l. b) The normalized voltage at f_c.

In this operation, it is proper to select m_a as 1 since the achievable voltage ranges for both frequencies are compatible at this point as can be seen in Fig. 2.a.

For that m_a is 1, the normalized voltages (over V_{DC}) of $\hat{V}_{ABf_c}$ and $\hat{V}_{ABf_l}$ are drawn in Fig. 4 for changing $\Delta\theta_c$ and $\Delta\theta_r$. It is observed that while the normalized voltages at f_C (f_2) can be adjusted in the range of [0, 0.601], the normalized voltages at f_L (f_1) can be adjusted in the range of [0 0.318]. The normalized voltage ranges are swapped if we use f_H instead of f_L. One of these two operations can be selected or switched online based on the required power ratings of the Rx sides.

D. Wideband Operation

In the wideband operation, the f_R component is used to achieve the lower frequency (f_1), and f_C is used to obtain the higher frequency component (f_2). The peak value of f_R and f_C can be calculated in the phasor domain by using (2) and (4), and they are given in (8) and (9).

$$\hat{V}_{ABf_r} = V_{DC}m_a\sqrt{\frac{1-cos(\Delta\theta_R)}{2}} \quad (8)$$

$$\hat{V}_{ABf_c} = V_{DC}\frac{2}{\pi}J_o(\frac{\pi}{2}m_a)\sqrt{1-cos(\Delta\theta_C)} \quad (9)$$

In this operation, it is proper to select m_a as 0.8 since the achievable voltage ranges for both frequencies are equal at this point, as can be seen in Fig. 2.a. For that m_a is 0.8, the normalized voltages (over V_{DC}) of $\hat{V}_{ABf_R}$ and $\hat{V}_{ABf_C}$ are drawn in Fig. 5 for changing the control parameters of $\Delta\theta_C$ and $\Delta\theta_R$. It is observed that both normalized voltages at f_R (f_1) and f_C (f_2) can be adjusted in the range of [0, 0.81].

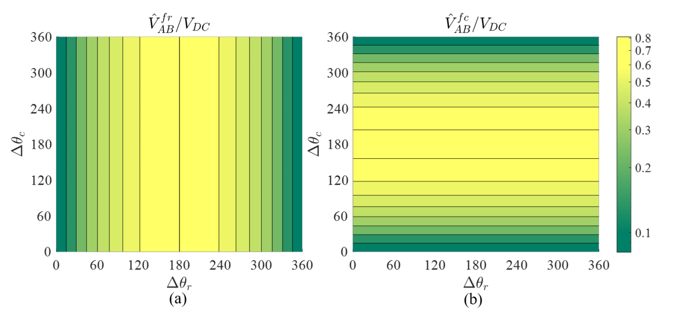

Fig. 5. Wideband Operation. a) The normalized voltage at f_R. b) The normalized voltage at f_C.

III. DISCUSSIONS AND FURTHER INVESTIGATIONS

A. Dual-Frequency Compensation System

A dual-frequency compensation system on the transmitter side operates at both frequencies, while series capacitors set the receiver sides to their respective resonant frequencies. This paper focuses specifically on dual-frequency excitation by using the modulation method, so we present the values and the type of compensation circuit employed rather than delving into the design of coil and compensation system, which can be found in the literature [15], [16]. Fig. 1 shows the diagram of dual-frequency compensation circuit, and Table II lists the circuit parameters of both wideband and narrowband operations.

TABLE II
DUAL-RECEIVER WPT SYSTEM PARAMETERS

Parameters		Simulation Value	Experimental Value
Transmitter Inductance	L_{TX}	$48\mu H$	$46.6\mu H$
Receiver Inductances	L_{RX1}	$75\mu H$	$75\mu H$
	L_{RX2}	$75\mu H$	$75\mu H$
Narrowband Compensation Inductance	L_{TX}	$1.5\mu H$	$1.517\mu H$
Wideband Compensation Inductance	L_{TX}	$28\mu H$	$26.8\mu H$
Narrowband Transmitter Compensation Capacitances	C_{TX1}	$454pF$	$463.3pF$
	C_{TX2}	$13.2nF$	$12.59nF$
Narrowband Recevier Compensation Capacitances	C_{RX1}	$340pF$	$334.5pF$
	C_{RX2}	$236pF$	$237.6pF$
Wideband Transmitter Compensation Capacitances	C_{TX1}	$31nF$	$30.8nF$
	C_{TX2}	$1nF$	$1nF$
Wideband Recevier Compensation Capacitances	C_{RX1}	$33nF$	$34.5nF$
	C_{RX2}	$236pF$	$237.6pF$
Narrowband Load Resistances	R_{L1}	68Ω	67.7Ω
	R_{L2}	68Ω	67.7Ω
Wideband Load Resistances	R_{L1}	4.7Ω	4.7Ω
	R_{L2}	68Ω	67.7Ω
Mutual Inductance	M_1	$6\mu H$	$6.2\mu H$
	M_2	$6\mu H$	$6.2\mu H$

B. Gain Response and the Interference between Receivers

The gain responses of receivers for narrowband and wideband operations are shown in Fig 6.

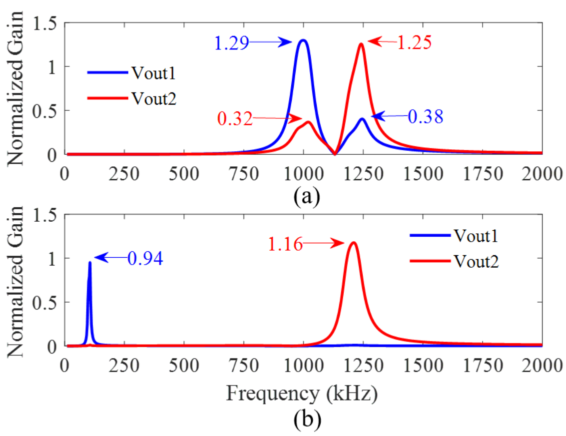

Fig. 6. Gain response of the dual receivers WPT system. a) Narrowband operation. b) Wideband operation.

Notably, while almost no interaction occurs between the receivers in a wideband operation, the narrowband operation introduces mutual influence. This influence changes the effective gain for dual-frequency excitation, so the operating phase shifts should be adjusted to account for this interference effect. Moreover, optimization of the compensation method or proper frequency selection can be recommended to mitigate this effect. For example, anti-interference compensation on the receiver sides might be suitable [17]. Additionally, the cross-coupling between receivers should be minimized, since it increases the interference ratio.

C. DC-link Utilization ratio of the Proposed Modulation Method

The proposed modulation allows for voltage control at two frequencies, which are limited to specific DC-link utilization ratio, which are given in Table III. The utilization ratios of the dual frequency excitation vary based on frequency selection in the other modulation techniques. In a system using superposition in SPWM, the summation of two signals should be at a maximum of 1 [13]. If you use antiphase signals, you can increase the utilization ratio. In the paper using SHEPWM, it is observed that the utilization ratio typically range between 0.3 and 0.9 [8]. Moreover, when two distinct frequencies are excited with two half-bridges, a utilization ratio of $0.5 \times 4/\pi = 0.64$ can be achieved for both frequencies. Our recommended wide-band modulation exceeds the gains of a two-half-bridge configuration. In the narrow band, one frequency could be excited with approximately these values while the other frequency component has a lower gain.

TABLE III
DC-LINK UTILIZATION RATIO OF THE PROPOSED MODULATION TECHNIQUE

	Voltage gain at f_1	Voltage gain at f_2
Wideband Operation	0.81	0.81
Narrowband Operation	0.318	0.601

D. Dual-receiver Output Regulation

The first control method in the proposed system is to adjust the carrier and reference phase shifts since you can change the voltage gain of the modulation. The second method is to detune the operating frequency since the proposed modulation technique can easily accommodate various frequencies. Furthermore, the active rectifiers at the receiver sides might be utilized to regulate the output voltages finely. In this paper, the control loop is not closed, and the output voltages have been controlled by introducing phase shifts.

E. Zero Voltage Switching Conditions

Conventional wireless power transfer (WPT) systems act as an inductive load, causing the current to lag when operating above the resonant frequency (unless in bifurcation condition). Before setting the gate signal high, a dead-time (blanking time) is given between each leg's top and bottom switches to prevent short-circuiting of the DC-link capacitors. During this dead-time period, the load current discharges the output capacitances of the switches. The inductive operation and lagged current ensure that the current direction always aligns with the discharging of the capacitors. As a result, the switches achieve zero-voltage switching (ZVS) at turn-on. However, in the proposed system, the existence of multi-frequency components in the transmitter current disrupts this assurance, even if the system operates in the inductive region at each frequency. Nevertheless, the proposed system may still have partial ZVS points, depending on the magnitudes and frequencies of the components of the Tx currents. An example operating point is depicted in Fig. 7, with the ZVS points marked.

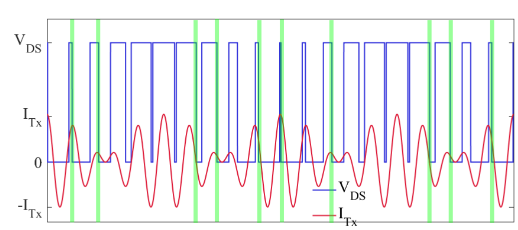

Fig. 7. Exemplary waveforms of drain-source voltage (V_{DS}) and transmitter current (I_{Tx}) with marked ZVS points in green. 10 of 20 turn-on instances achieve ZVS.

Therefore, the system needs to be designed assuming hard-switching conditions. This design remains in the worst-case scenario. However, the efficiency might be higher in practical use than calculated, thanks to the partial ZVS.

F. Efficiency Analysis

The system's power losses are primarily due to the losses of inverter (P_{inv}), rectifier (P_{rec}), and network (P_{net}) as given in [18]. Then, overall system efficiency can be calculated by

$$\eta = \frac{P_{out}}{P_{in}} = \frac{P_{out}}{P_{out} + P_{inv} + P_{rec} + P_{net}} \tag{10}$$

where P_{in} is input power , and P_{out} is output power. Firstly, the inverter loss can be split into two parts as given in

$$P_{inv} = P_c + P_{sw} \tag{11}$$

where P_c is the conduction loss, and P_{sw} is the switching loss. In conventional 1Tx-1Rx WPT systems, achieving zero voltage switching (ZVS), which reduces switching losses significantly, is ensured by operating in the inductive region near the zero-phase angle (ZPA). Then, the inverter loss, when in ZVS operation, can be considered conduction loss. However, in the proposed 1Tx-2Rx system, the ZVS might not be ensured, and the inverter loss should be calculated in hard-switching operation, as given by

$$P_{inv} = P_c = {I_{Tx}}^2 r_{ds} + f_{sw}(E_{sw-ZCS} + E_{sw-OL}) \tag{12}$$

where I_{Tx} is the RMS value of the Tx current, r_{ds} is the MOSFET on-state resistance, f_{sw} is the switching frequency, E_{sw-ZCS} is the zero current switching energy due to output capacitances of the switches, and E_{sw-OL} is the overlapping switching energy because of switching speed of switches as dv/dt and di/dt. Moreover, operating near ZPA can also decrease conduction losses by lowering the RMS of the Tx current since the power factor becomes unity. Secondly, the rectifier operates in continuous conduction mode, resulting in pure sinusoidal current. Therefore, the loss can be calculated by

$$P_{rec} = \left(\frac{2\sqrt{2}}{\pi} V_F I_{Rx1} + r_F I_{Rx1}^2\right) + \left(\frac{2\sqrt{2}}{\pi} V_F I_{Rx2} + r_F I_{Rx2}^2\right) \tag{13}$$

where V_F and r_F are the opening voltage and on-state resistance of the diodes, and I_{Rx1} and I_{Rx2} are receiver currents. Lastly, the loss from network elements, such as passive elements like coils and capacitors, depends on the RMS value and frequency of the currents of the Tx and Rx sides. The loss can be calculated by

$$P_{net} = I_{Tx}^2 r_{net_{Tx}} + I_{Rx1}^2 r_{net_{Rx1}} + I_{Rx2}^2 r_{net_{Rx2}} \tag{14}$$

where $r_{net_{Tx}}$, $r_{net_{Rx1}}$ and $r_{net_{Rx2}}$ are the representative resistances for network losses for the Tx and Rx sides.

The analysis conducted above shows that the proposed system might have higher inverter loss than conventional 1Tx-1Rx systems due to the absence of ZVS. The other losses are almost equal to those of conventional systems if we make a fair comparison. Yet, the incorporation of wideband gap semiconductors plays a crucial role. It allows for an increase in the dv/dt, thereby reducing switching losses and enabling hard-switching opportunities at higher switching frequencies. Consequently, the overall system may have a switching loss that forms a minority portion of the total loss. In such a scenario, reducing costs achieved by decreasing the number of inverters can offset the efficiency decrease due to switching loss.

IV. Experimental Validation

An experimental setup, shown in Fig. 8, is established to validate the proposed system. The system parameters are shown in Table II. In the setup, we wound the coils using 1mm diameter litz wires. The oscilloscope was a 6-channel Tektronix MSO46. We employed PEM CWTMini HF03B current probes for AC current measurement and Tektronix THDP0100 differential probes for voltage measurement. The power supply was an Agilent N8739A. To generate the proposed modulation, the TI C2000 TMS320F28379D microcontroller is utilized.

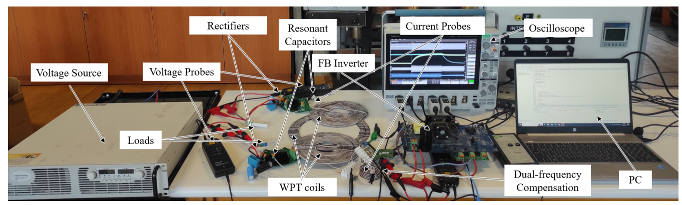

Fig. 8. Experimental setup of Dual-mode WPT System.

A. Dual-Mode Inverter Tests

The voltage waveforms of V_{AB} for both narrowband and wideband operations are shown in Fig. 9 and Fig. 10. As expected, it is observed that the voltages of each frequency can be independently controlled by $\Delta\theta_R$ and $\Delta\theta_C$. There are slight differences between experimental results and mathematical calculations, which are at a maximum of 6%.

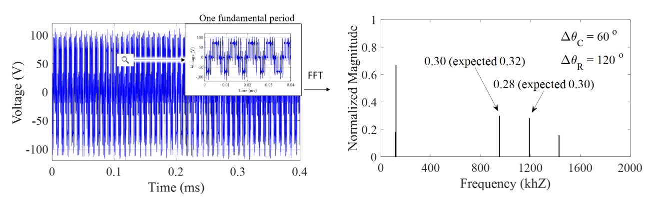

Fig. 9. Inverter Output Voltage and its harmonics spectrum for narrowband operation. The fundamental frequency is 119.5 kHz, and the switching frequency is 1190 kHz. The modulation index is 1.

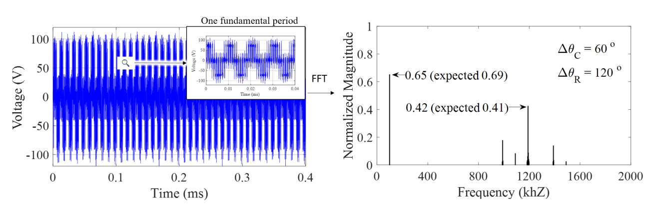

Fig. 10. Inverter Output Voltage and its harmonics spectrum for Wideband Operation. The fundamental frequency is 100kHz, and the switching frequency is 1190khZ. The modulation index is 0.8.

B. Dual-Mode WPT System Tests

The Rxs and outputs' currents and V_{AB} voltage are obtained for narrowband and wideband operations, as given in Fig. 11 and Fig. 12. Transient analysis was performed to study the impact of different operating phase shifts in both wideband and narrowband operations. It's important to note that the voltages in this experimental setup may deviate slightly from the analytical calculations due to dead time and other nonlinearities since closed-loop control was not utilized. Furthermore, in narrowband operation, the interference between receivers necessitates minor updates to the phase shifts in addition to the analytical calculations in order to compensate for the effect.

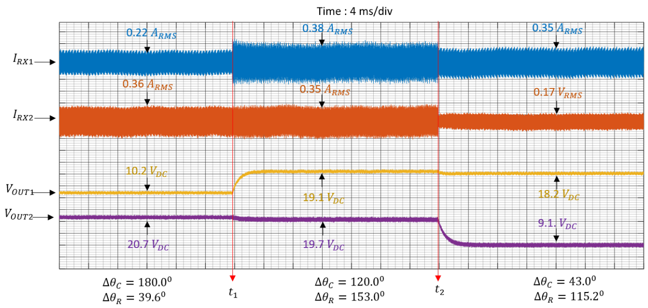

Fig. 11. Narrowband operation of dual-mode WPT system. m_a is 1, f_L is 951 kHz, and f_C is 1190 kHz.

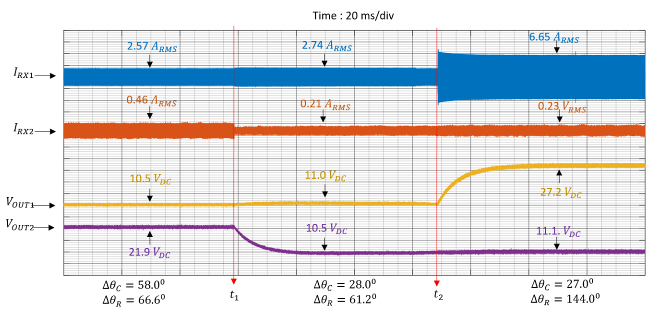

Fig. 12. Wideband operation of dual-mode WPT system. m_a is 0.8, f_R is 100 kHz, and f_C is 1190 kHz.

C. Dual-Mode WPT System Power Transfer Efficiencies

The efficiency measurements for both narrowband and wideband operations in various conditions are provided in Table IV. In all cases, it was observed that the efficiencies were about 75%. Our proposed system has a key advantage that could potentially lead to increased efficiency by reducing the required switching frequencies. Still, it is also worth considering optimizing the coil and compensation systems to improve efficiency further.

TABLE IV
THE POWER TRANSFER EFFICIENCIES FOR DIFFERENT OPERATING POINTS

	Carrier Phase Shift	**Reference Phase Shift**	**Power Transfer Efficiency**
Narrowband Operation	180°	39.6°	74.6 %
	120°	153°	76.3 %
	43°	115.2°	76.0 %
Wideband Operation	58°	66.2°	75.3%
	28°	61.2°	75.7 %
	27°	144.0°	75.5 %

V. Comparison with Literature

Existing studies are compared with the proposed system in Table V. Unlike the approaches presented in [7] and [14], our proposed system does not require extra switches, which reduces the cost and complexity. In contrast to the system discussed in [13], our system allows both wideband and narrowband operations and has operating frequencies near the switching frequency, decreasing switching losses. Unlike the method outlined in [8], our system does not require an offline algorithm to calculate the different quiescent points, thereby enabling dynamic operations.

TABLE V
COMPARISON WITH EXISTING STUDIES IN THE LITERATURE.

	Channel Mode	**Tx Device**	**Offline Algorithm**	**Operating Frequency**
[7]	2 (WB)	Two-2LC	NR	$= f_s$
[8]	2 (NB/WB)	Single-2LC	R	$\leq f_s$
[13]	2 (NB)	Single-2LC	NR	$< f_s$
[14]	2 (NB)	Single-MLI	NR	$\geq f_s$
This work	2 (NB/WB)	Single-2LC	NR	$= f_s$

2LC : Two level converter, **MLI** : Multi level inverter,
NB : Narrowband, **WB** :Wideband, **R** : Required, **NR** :Not required.

VI. Conclusion

In this letter, concurrent power transfer at dual frequency was achieved by a single converter using a novel hybrid reference and carrier phase shifts method of SPWM, allowing for a controllable dual-frequency output. This versatile modulation method is applicable to narrowband and wideband operations, and it enables the use of single Tx device by multiple standards. The experimental setup was established to confirm the effectiveness of the proposed modulation technique, and a good agreement was observed between experimental results and mathematical calculations. Further, the proposed system offers several advantages, such as reduced switching components and lower switching frequency, resulting in increased efficiency and decreased system cost. Consequently, the proposed system enhances the adoption of dual-band WPT systems that support multi-standard usage in robotics and consumer electronics.

References

[1] W. Jin, A. T. L. Lee, S.-C. Tan, and S. Y. R. Hui, "Single-inductor multiple-output inverter with precise and independent output voltage regulation," *IEEE Transactions on Power Electronics*, vol. 35, no. 10, pp. 11 222–11 234, 2020.

[2] "The qi wireless power transfer system power class 0 specification," Apr. 2016, [online] Available: https://www.wirelesspowerconsortium.com/.

[3] "Nxp wireless power solutions," *NXP, May-2017. [Online]. Available: https://www.nxp.com/docs/en/supporting-information/BL-Micro-NXP-Wireless-Charging-Solutions-Beta-Chen.pdf.*, [Accessed: 20-Mar-2023].

[4] Y. Xiao, C. Liu, Y. Huang, and S. Liu, "Concurrent wireless power transfer to multiple receivers with additional resonant frequencies and reduced power switches," *IEEE Transactions on Industrial Electronics*, vol. 67, no. 11, pp. 9292–9301, 2020.

[5] J. Wu, L. Bie, W. Kong, P. Gao, and Y. Wang, "Multi-frequency multi-amplitude superposition modulation method with phase shift optimization for single inverter of wireless power transfer system," *IEEE Transactions on Circuits and Systems I: Regular Papers*, vol. 68, no. 5, pp. 2271–2279, 2021.

[6] A. wireless power transfer system baseline system specification (BSS), *Standard A4WP-S-0001 v1.3*, Jan. 2014.

[7] D. Ahn and P. P. Mercier, "Wireless power transfer with concurrent 200-khz and 6.78-mhz operation in a single-transmitter device," *IEEE Transactions on Power Electronics*, vol. 31, no. 7, pp. 5018–5029, 2016.

[8] C. Zhao and D. Costinett, "Gan-based dual-mode wireless power transfer using multifrequency programmed pulse width modulation," *IEEE Transactions on Industrial Electronics*, vol. 64, no. 11, pp. 9165–9176, 2017.

[9] F. Liu, Y. Yang, Z. Ding, X. Chen, and R. M. Kennel, "A multifrequency superposition methodology to achieve high efficiency and targeted power distribution for a multiload mcr wpt system," *IEEE Transactions on Power Electronics*, vol. 33, no. 10, pp. 9005–9016, 2018.

[10] Z. Liu, M. Su, Q. Zhu, Y. Chao, S. Zang, and A. P. Hu, "A dual-frequency three-dimensional wpt system with directional power transfer capability at two separately regulated outputs," *IEEE Journal of Emerging and Selected Topics in Power Electronics*, pp. 1–1, 2022.

[11] C. Qi, S. Huang, X. Chen, and P. Wang, "Individual output voltage regulation method of multifrequency multireceiver simultaneous wpt systems with a single inverter," *IEEE Journal of Emerging and Selected Topics in Power Electronics*, vol. 11, no. 1, pp. 1245–1261, 2023.

[12] W. Jin, A. T. L. Lee, S.-C. Tan, and S. Y. Hui, "A gallium nitride (gan)-based single-inductor multiple-output (simo) inverter with multi-frequency ac outputs," *IEEE Transactions on Power Electronics*, vol. 34, no. 11, pp. 10 856–10 873, 2019.

[13] C. Xia, N. Wei, H. Zhang, S. Zhao, Z. Li, and Z. Liao, "Multifrequency and multiload mcr-wpt system using hybrid modulation waves spwm control method," *IEEE Transactions on Power Electronics*, vol. 36, no. 11, pp. 12 400–12 412, 2021.

[14] Y. Liu, C. Liu, X. Gao, and S. Liu, "Design and control of a decoupled multichannel wireless power transfer system based on multilevel inverters," *IEEE Transactions on Power Electronics*, vol. 37, no. 8, pp. 10 045–10 060, 2022.

[15] Z. Zhang, X. Li, H. Pang, H. Komurcugil, Z. Liang, and R. Kennel, "Multiple-frequency resonating compensation for multichannel transmission of wireless power transfer," *IEEE Transactions on Power Electronics*, vol. 36, no. 5, pp. 5169–5180, 2021.

[16] C. Qi, H. Miao, Z. Lang, and X. Chen, "A generalized methodology to generate, amplify and compensate multi-frequency power for a single-inverter-based mf-mr-s-wpt system," *IEEE Access*, vol. 8, pp. 181 513–181 525, 2020.

[17] X. Tian, J. Zhang, H. Wang, and S. M. Goetz, "Design and analysis of automatic modulation and demodulation strategy in wireless power and drive transfer system," *IEEE Transactions on Industrial Electronics*, pp. 1–10, 2024.

[18] H. Liu, L. He, and B. Cheng, "Powerless fractional-order tuning wireless power transfer system with zero phase angle input," *IEEE Transactions on Circuits and Systems I: Regular Papers*, pp. 1–10, 2024.